QUARTERLY JOURNAL OF THE ROYAL METEOROLOGICAL SOCIETY
Q. J. R. Meteorol. Soc. **136(s1)**: 141–158 (2010)
Published online 26 January 2010 in Wiley InterScience
(www.interscience.wiley.com) DOI: 10.1002/qj.555

Links between African easterly waves, midlatitude circulation and intraseasonal pulsations of the West African heat low

C. Lavaysse,[a]* C. Flamant[a], S. Janicot[b] and P. Knippertz[c]
[a]*LATMOS, CNRS and Université Pierre et Marie Curie, Paris, France*
[b]*LOCEAN, IRD and Université Pierre et Marie Curie, Paris, France*
[c]*School of Earth and Environment, University of Leeds, UK*

ABSTRACT: During summer 2006, the intensity of the thermal depression over the Sahara, derived from European Centre for Medium-range Weather Forecast analyses, exhibited a strong decrease during the first couple of weeks of September. Simultaneously, widespread convective activity over the Sahel was detected. The aims of this study are to identify the reasons for this decrease of the West African Heat Low (WAHL) activity, to discuss the possible relationship with convection and to assess the representativity of such an event at the climatological time-scale. From spectral analysis of the daily WAHL thickness during summer 2006, two period bands of significant intraseasonal pulsations were identified, and confirmed using the ERA-40 reanalysis, namely 3–10 d and 10–30 d. In both the 2006 case-study and the climatological composite study, we find that detrimental conditions in the 3–10 d period band are associated with moist and cool advections in the lower troposphere linked to the southerly sector of African easterly waves (AEWs) which increase convective activity over the Sahel. These humid and cold advections from the south are more pronounced when the AEW interacts with a midlatitude depression. In the 10–30 d period band, the impact of midlatitude circulation is demonstrated. During the collapsing period of the 10–30 d pulsations of the WAHL thickness, an upper-level trough is seen over northern West Africa. This situation generates a surge of 700 hPa cold air from Libya into the Sahara, an increase of the 925 hPa anticyclonic circulation and a significant increase of convective activity over the Sahel. Copyright © 2010 Royal Meteorological Society

KEY WORDS West African monsoon; tropical convection; AMMA; ECMWF ERA-40 reanalyses; satellite-derived brightness temperature

Received 15 December 2008; Revised 28 October 2009; Accepted 5 November 2009

1. Introduction

Over West Africa, the intensity and the direction of low-level winds, such as the monsoon and the harmattan flows, are closely linked to the surface pressure gradient. These winds converge to the area of the lowest pressures, the Intertropical Discontinuity (ITD). During the summer, a low-level thermal depression, the so-called West African Heat Low (WAHL), which covers the warm and dry region of the Sahara, also contributes to decrease the surface pressure (Lavaysse *et al.*, 2009, LA09 hereafter).

In the mid-troposphere, the anticyclonic circulation associated with the WAHL as well as the meridional gradient of temperature between the rain belt and the WAHL contribute to increase and maintain the African Easterly Jet (AEJ; Thorncroft and Blackburn, 1999). Using an idealized heat low model, Spengler and Smith (2008) have shown the development of the upper-level anticyclone above the anomaly of temperature. In the model, the anticyclone extends through much of the troposphere, but has a maximum strength in the lower troposphere (around 3 km). The northerly wind associated with the divergent flow of the WAHL at 700 hPa generates a shallow meridional overturning circulation (Trenberth *et al.*, 2000). This return flow has been confirmed using sounding observations (Zhang *et al.*, 2006).

Several studies have highlighted the important role of the seasonal cycle of the WAHL on the West African monsoon system, and particularly on the so-called monsoon onset (e.g. Sultan *et al.*, 2003; Ramel *et al.*, 2006; LA09). The WAHL commonly interacts with both the monsoon system (to the south) and the Mediterranean basin (to the north). To the south, Parker *et al.* (2005) have suggested that the southerly advection of moist cool monsoon flow, larger along the eastern fringe of the WAHL than along the western fringe, is likely to enhance the probability of cloud cover poleward of the main precipitation zone. The decrease of temperature in this area (following a monsoon surge) creates conditions detrimental to the existence of a vigorous WAHL. More recently, Couvreux *et al.* (2009) have provided some evidence of coupling between the WAHL and the monsoon flow at intraseasonal scales during a short time sequence of the 2006 pre-onset period. To the north, Chauvin *et al.* (2009)

*Correspondence to: C. Lavaysse, Université Pierre et Marie Curie, 4 Place Jussieu, 75252 Paris Cedex 05, France. E-mail: christophe.lavaysse@aero.jussieu.fr

have detected intraseasonal variability in the 850 hPa temperature field over the northern part of West Africa. Their results show the possible interaction between the temperature at low levels over West Africa (as a proxy for the WAHL activity shown by LA09) and the midlatitude circulation. Finally, surges of cold air from the Mediterranean, upon reaching the African continent, also tend to break the African monsoon system (Vizy and Cook, 2009).

However, to date, no investigation has been made of the impact of the specific WAHL pulsations at the intraseasonal time-scale on the low-level wind field and on convection during the rainy season (i.e. the mature monsoon period), when the location of the WAHL is stationary west of the Hoggar.

Thus the aims of this study are to characterize the intraseasonal oscillations of the WAHL and to better understand their dynamical environment over West Africa as well as the associated convective activity during the summer. We shall use both a case-study from the African Monsoon Multidisciplinary Analysis project (AMMA; Redelsperger *et al.*, 2006) Special Observation Period (SOP) that took place in 2006 and a composite study based on the European Centre for Medium-range Weather Forecast (ECMWF) ERA-40 reanalysis. We will focus on the possible relationship between the WAHL pulsations and other key synoptic components of the West African monsoon system presented now.

African easterly waves (AEWs) are known to be an important feature of the West African monsoon system with a strong impact on convection (Burpee, 1972; Duvel, 1990; Diedhiou *et al.*, 1998, 1999). These 3–5 d waves propagate westward along both flanks of the African Easterly Jet (AEJ) and can provide a favourable environment for generating rainfall especially over the Sahel (Fink and reiner, 2004; Mathon *et al.*, 2002). A second type of atmospheric wave has been pointed out by Viltard *et al.* (1997) and Diedhiou *et al.* (1999). These waves are different from the 3–5 d AEWs. Their period is about 6–9 d and their wavelength is around 5000 km. They are located further north than the 3–5 d AEWs (i.e. over the Sahara desert). Their impact on convection is not yet understood. But, as for the 3–5 d AEWs, the modification of the low-level winds (i.e. associated with the succession of southerly and northerly wave sectors) and the modification of low-level instability associated with the cyclonic and anticyclonic circulation could favour or inhibit the convective activity. Cuesta *et al.* (2009) have shown that these waves could be associated with rainfall events in Tamanrasset (Algeria), in the southeastern part of the Sahara. Leroux and Hall (2009) have shown that the favourable environment for the development of strong AEWs are a strong AEJ, a strong vertical wind shear and a strong and extended potential vorticity reversal.

At lower frequencies, i.e. between 10 and 60 d, Sultan *et al.* (2003) have identified intraseasonal variability of rainfall over the Sahel usually close to 15 d, associated with large and coherent anomalies in the 925 hPa wind field. Based on a composite study, they found the wet phases over the Sahel to be linked with wide southerly anomalies of the wind, as well as a weakened AEJ and increased AEW activity (Lavaysse *et al.*, 2006). They could be related to Rossby waves (Kiladis and Weickmann, 1997; Matthews, 2004).

Tropical–extratropical interactions can also modify the large-scale structure of the wind field over West Africa and generate an increase of convective activity. Potential vorticity intrusion, cut-off lows, or the crossing of midlatitude depression can interact with AEWs (Nicholson, 1981). The cut-off lows are a common feature of Mediterranean meteorology, especially in warm months where they are associated with cyclonic circulation (Porcu *et al.*, 2007). Several studies have observed extreme precipitation associated with these extratropical–tropical interactions over Algeria or Morocco (Fink and Knippertz, 2003; Knippertz *et al.*, 2003). The authors have observed large-scale convective activity associated with unstable dynamical features and potential vorticity intrusion, which is defined as a tropical plume event. These events could affect a large part of West Africa (Knippertz, 2005; Knippertz and Martin, 2005). A case of cold air outbreak from Europe penetrating into West Africa has also been studied by Thorncroft and Flocas (1997). They have observed equatorward transport of cold air at 850 hPa from midlatitudes in February 1988 associated with a cold front passage. Nevertheless, the interactions with other African monsoon components, such as AEJ, were weaker in the winter case described by Thorncroft and Flocas (1997) than in our study.

Finally, the interaction between the midlatitude circulation and heat lows has also been studied over the Australian continent. Spengler *et al.* (2005) have clarified the relationship between the heat trough and the development of a subtropical front using an idealized model, but also the possible distortion of the heat low by the background flow. They show that horizontal wind shear leads to the deformation of the heat low. Smith *et al.* (1995) have detailed a case of penetration of three cold fronts into the subtropical region in Australia, which eventually merged with the Australian heat low. Even though their case-study took place during the dry season (May–October), it suggests the possible dynamical effect of the upper-level trough onto the heat trough in the lower troposphere. Hanstrum *et al.* (1990) presented a climatology of events, frequently occurring during the spring, where the wind field ahead of cold fronts leads to modify the heat low.

The main difference between these previous studies and this one is the season. Our study is based on the summer season over West Africa, during the rainy season in the Sahel, whereas the previous study analyse these interactions during the winter or spring seasons.

During summer 2006, the intensity of the WAHL over the Sahara (as derived from ECMWF analyses), exhibited a strong decrease during the first couple of weeks of September. This event generated the shallowest WAHL of summer 2006. At the same time, widespread convective activity and positive rainfall anomaly over the northern part of the Sahel were detected. The aims of this study

are to identify the reasons of this decrease of the WAHL activity, discuss the possible relationship with convection and rainfall, and assess the representativity of such an event at the climatological time-scale.

The paper is organized as follows. The data used in this study are presented in section 2. Then, the intraseasonal oscillations of the WAHL in 2006 will be detailed in section 3. These results will be compared to the climatological analysis of the 10–30 d and 3–10 d period band oscillations in section 4 and 5 respectively. In section 6, we summarize and conclude.

2. Dataset and method

In this study, only the satellite period of the ECMWF ERA-40 reanalysis data, i.e. from 1979 to 2001, has been used. It is generally regarded as the more reliable part of the dataset for climatological analysis (Kållberg *et al.*, 2005). The model variables are available on 23 pressure levels between 1000 and 1 hPa, with a horizontal resolution of $1.125^\circ \times 1.125^\circ$. The following fields have been used in this study: the three components of the wind, moisture, and temperature. As explained in LA09, only values at 0600 UTC have been used. This choice is motivated by the fact that turbulent mixing is weakest in the planetary boundary layer while low-level winds are strongest at this time. For the year 2006, we have used the operational analysis from ECMWF with the same spatial and temporal resolution.

There exist very few observational datasets to evaluate the model-based climatological studies. In this study, we have used brightness temperature data from the Cloud Archive User Service (CLAUS; http://badc.nerc.ac.uk/data/claus/), funded by the European Union, to look into climatological patterns of near-surface temperatures as well as convection. The CLAUS project maintains a long time-series of three-hourly thermal infrared images of the Earth based on the level B3 10 μm radiances from operational meteorological satellites participating in the international Satellite Cloud Climatology Programme (ISCCP, Brest *et al.*, 1997).

The CLAUS archive currently spans the period 1984 to 2004. In this work, the infrared (IR) brightness temperature fields have been interpolated onto a regular horizontal grid at the spatial resolution of $0.5^\circ \times 0.5^\circ$. To estimate the convective activity, we compute an index based on the daily number of pixels below 230 K using the eight images available per day. This threshold allows to identify deep convection over West Africa (Fu *et al.*, 1990).

Moreover, to assess the convective activity in 2006, we have used hourly images acquired at 10.8 μm by the Spinning Enhanced Visible and InfraRed Imager (SEVIRI) on board the Meteosat Second Generation (MSG) satellite. The data comes from the 'AMMA satellite' database archived at the Institut Pierre-Simon Laplace (IPSL), Paris. To obtain a regular grid over West Africa, the brightness temperature has been averaged over $0.04 \times 0.04^\circ$ square boxes.

The rainfall is given by the Global Precipitation Climatology Project (GPCP; http://www.gewex.org/gpcp.html). Using multi-satellite data (satellite geostationary and low-orbit infrared, passive microwave) and a combination with observations (rain-gauges, soundings) the 1DD (1 degree daily) version provides a daily global $1^\circ \times 1^\circ$ grid field of total surface precipitation.

Using the same methodology as in LA09, we detect the WAHL location using the low-level atmospheric thickness (LLAT) which is defined by the difference between two geopotential heights. The upper boundary is located at 700 hPa, corresponding to the limit below which upward motion as is seen in the model. The lower boundary is chosen at 925 hPa, not to be affected by topography below 800 m above mean sea level. The WAHL is defined as the area associated with 10% of the largest LLAT over West Africa. Figure 1(a) displays the mean occurrence frequency of the WAHL location during the summer season of 2006 (averaged between 20 June to 17 September). The location of the WAHL appears quite stationary during this period, with more than 90% of occurrence frequencies in the centre of the area. Moreover, it is worth noting the consistency between the location of this low-level depression and the 925 hPa wind field averaged over the entire summer (indicated by vectors) with the cyclonic circulation located over the maximum of the WAHL detection.

To characterise the WAHL activity during the summer season, we calculate the average of the LLAT within the area covered by the WAHL. Large LLATs are associated with deep or deepening WAHL whereas small LLATs are indicative of a shallow or collapsing WAHL.

To separate significant signal from random fluctuations, we applied a Student test of each composite study. All results displayed in this study have a significance higher than 0.8.

3. Intraseasonal oscillations of the WAHL in 2006

3.1. The August–September 2006 case-study

We have analysed the temporal evolution of the WAHL thickness during the AMMA SOP in the summer 2006 (Redelsperger *et al.*, 2006; Lebel *et al.*, 2009) especially when the WAHL is located over the Sahara (LA09). As discussed in the following, during this period the WAHL exhibited pulsations (i.e. fluctuations of its depth) at different time-scales (Figure 1(b)).

Between 27 August and 7 September 2006, an abrupt decrease of the WAHL thickness is observed, generating the weakest WAHL recorded during the 1 June–1 October period. During the same period, imagery from SEVIRI 10.8 μm channel indicates widespread convective activity over the Sahel and the Sahara from 4 to 7 September (Figure 2). This increase of convective activity is accompanied by an increase of rainfall north of 20°N (as indicated by GPCP, not shown).

In order to identify the significant period of temporal pulsations of the WAHL in the summer of 2006, we

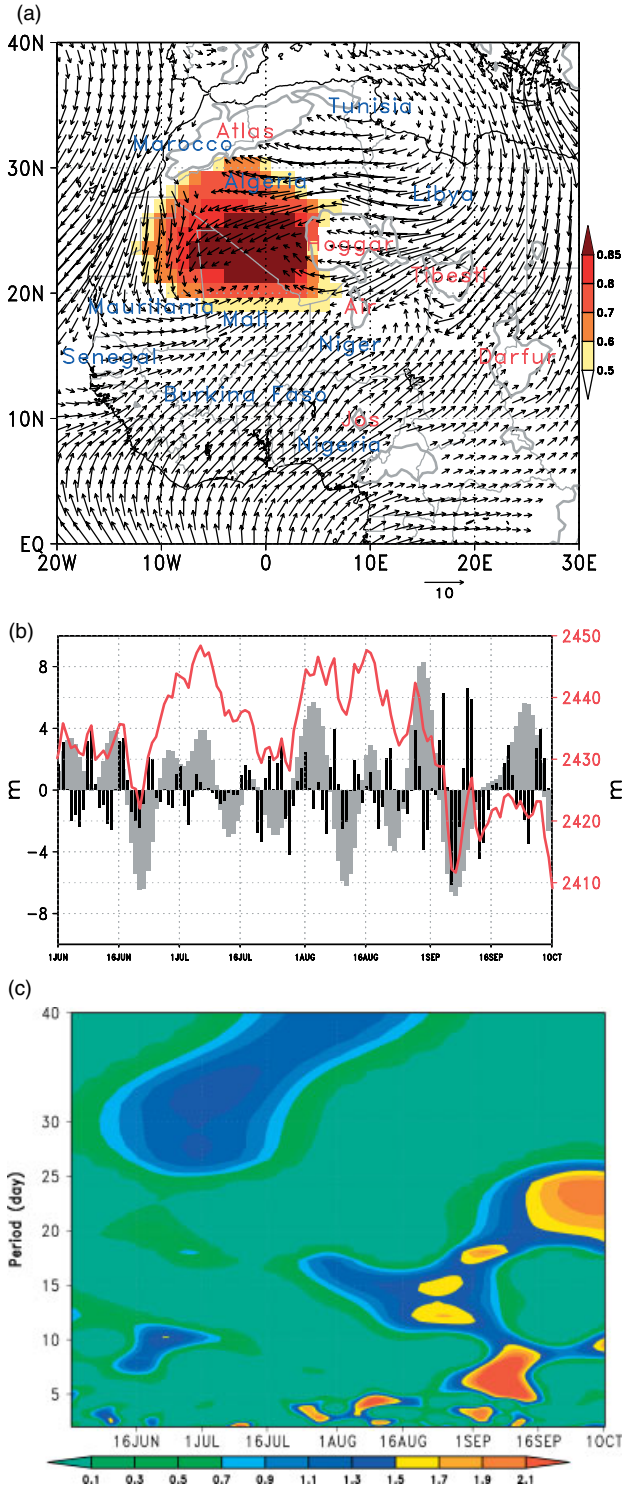

Figure 1. (a) Mean occurrence frequency of the WAHL (shading) in the summer of 2006 (see text for more details), with superimposed mean wind field at 925 hPa ($m\,s^{-1}$, vectors). (b) Temporal evolution of the thickness of the WAHL in 2006 (m, solid line, right y-axis). Bars indicate filtered thickness (m, left y-axis) in the 10–30 d period band (light bars) and in the 3–10 d period band (dark bars). (c) Wavelet analysis based on a Morlet mother wave of the WAHL thickness in summer 2006 (s^{-1}).

have performed a wavelet analysis, based on a Morlet mother wave (Torrence and compo, 1998). The result of the wavelet analysis shows two significant pulsation periods (Figure 1(c)). A first pulsation period is observed below 10 d and is associated with the abrupt decrease of the WAHL thickness during the first week of September (black bars in Figure 1(b)). A second pulsation period (periods between 15 and 25 d) appears to have a significant influence on the WAHL variability at the beginning of September (grey bars in Figure 1(b)). To assess whether the results found for 2006 were representative, we also have performed a wavelet analysis of the thickness of the WAHL during the summer season for the entire ERA-40 period (1979–2001, not shown). As in 2006, the wavelet analysis revealed the existence of the same two distinct and significant time-scales of pulsation. The first, under 10 d, could be related to quick pulsations like both 3–5 and 6–9 d periods of the AEWs (Diedhiou *et al.*, 1998, 1999). The second one, between 15 and 25 d, could be linked with larger-scale anomalies like the intraseasonal pulsation of the monsoon flow (Sultan *et al.*, 2003).

To focus on these two period bands, and to analyse their possible relationship with other synoptic components of the West African monsoon system, the time series of daily WAHL thickness has been filtered using a band-pass Kaiser filter (Kaiser and Reed, 1977). The filtered 10–30 d periods of the WAHL (grey bars in Figure 1(b)) are strong in June and from the beginning of August to the end of September. The filtered 3–10 d period band of the WAHL (black bars) are detected during the whole of the rainy season with a maximum intensity in September.

We now focus on the period between 28 August (when the WAHL is deep) and 7 September (when the WAHL becomes shallow) and analyse the origin of both 3–10 d and 10–30 d fluctuations of the WAHL thickness.

3.2. Investigation of the WAHL and synoptic environment variability in the 10–30 d period

The large-scale environment of the WAHL during this period is investigated on the basis of the anomalies of LLAT, the wind field at 700 hPa, and the 300 hPa geopotential height (Figure 3). The anomalies are computed independently for each grid box with respect to mean fields averaged over one period of the 10–30 d period pulsation (i.e. 22 August and 7 September). Whereas a maximum of WAHL activity is observed on 28 August (Figure 3(a)), in the 10–30 d period the maximum occurs on 30 August. The WAHL is then seen to collapse between 1 and 5 September (Figures 3(b)–(d)), and to exhibit a minimum of activity on 7 September (Figure 3(f)).

During the strengthening period of the WAHL (before 28 August, not shown), a warm and positive anomaly of LLAT develops along the eastern edge of the Mediterranean which propagates southward. This positive anomaly reaches Algeria on 26 August and is associated with an increase of brightness temperature at 10.8μm as observed with SEVIRI (Figure 2(c)). Then, on 28 and 30 August, the positive anomaly of LLAT moves westward (Figure 3(a)) and is associated with an increase of the WAHL thickness shown in Figure 1(b).

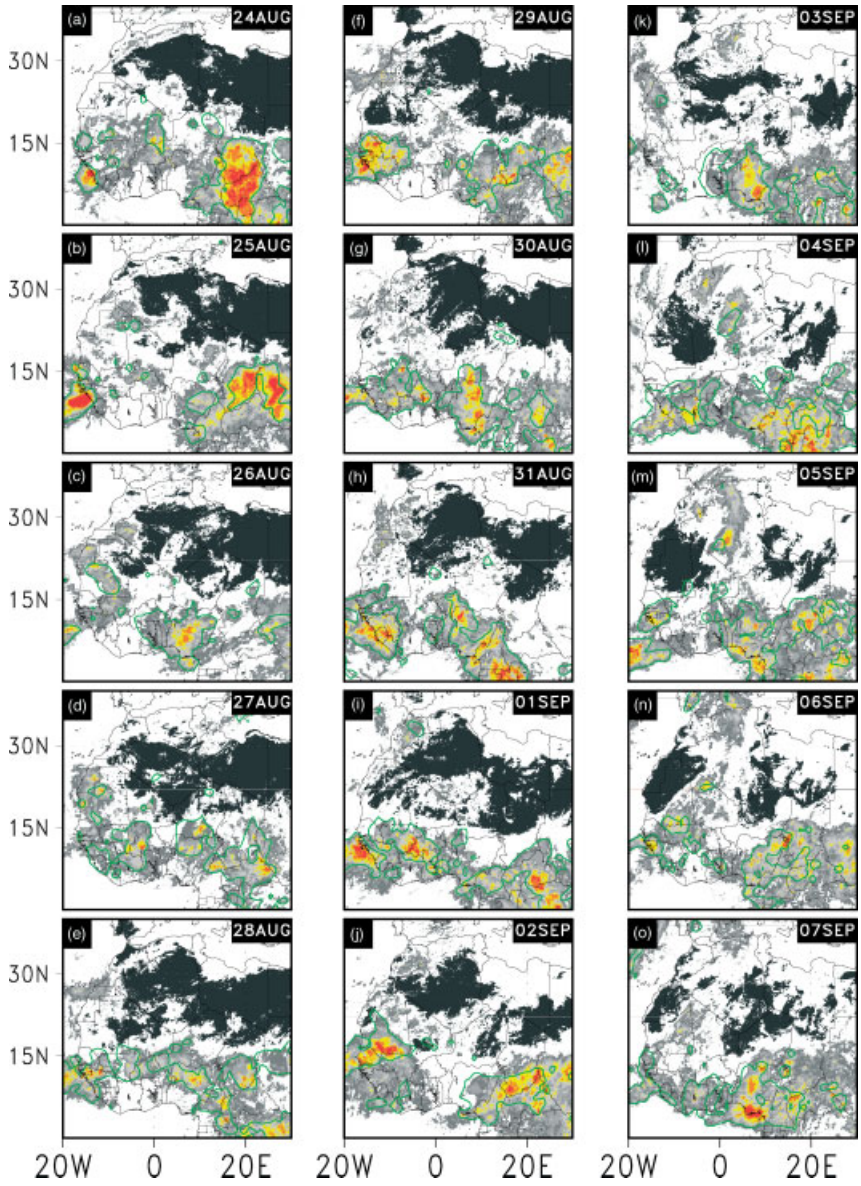

Figure 2. Sequence between (a) 24 August and (o) 7 September of the mean daily brightness temperature at 10.8 μm from SEVIRI over West Africa. Dark shading indicates regions of high brightness temperature (larger than 320 K), and light shading indicates regions of low brightness temperature (less than 220 K). Solid contours show 8 mm of daily accumulated rainfall from GPCP.

On 30 August, a cold depression is visible over Europe (Figure 3(b)) which reaches the eastern Mediterranean on 1 September (Figure 3(c)). At 300 hPa, we note a slight southeastward displacement of the negative geopotential height anomaly over the eastern Mediterranean (associated with the cold depression in the low troposphere).

On 3 September, the low positive anomaly of the LLAT and the 700 hPa anticyclone is centred over Morocco. The associated northeasterly wind over Algeria and Libya favours the development of the negative anomaly of LLAT (Figure 3(d)). The cold depression seems to trim the northern edge of the WAHL, which starts its southwestward displacement. This interaction between heat low and cold front has been illustrated over Australia by Smith *et al.* (1995), where the authors observe the collapsing and the displacement of the heat trough associated with the crossing of the cold front (Figure 2 in Smith *et al.*, 1995). Over Algeria, the penetration of relatively cold and humid air is associated with convective activity (e.g. on 3 September; Figure 2(k) and (l)). On 5 September, over the Mediterranean, a minimum of 300 hPa geopotential height tears off from the midlatitude circulation over Europe and generates a cut-off low circulation which reaches West Africa (Figure 3(e)). This upper-level depression generates a decrease of the 700 hPa geopotential height which, in turn, decreases the LLAT. As a result, the WAHL is detected more to the southwest than in the climatology of LA09. The convective activity increases in the area where the upper-level depression is seen. On 6 and 7 September, the negative geopotential anomaly in the upper levels moves westward and reaches the West African coast (Figure 3(f)). This is accompanied by a southwest to northeast oriented band of convection, as seen in Figures

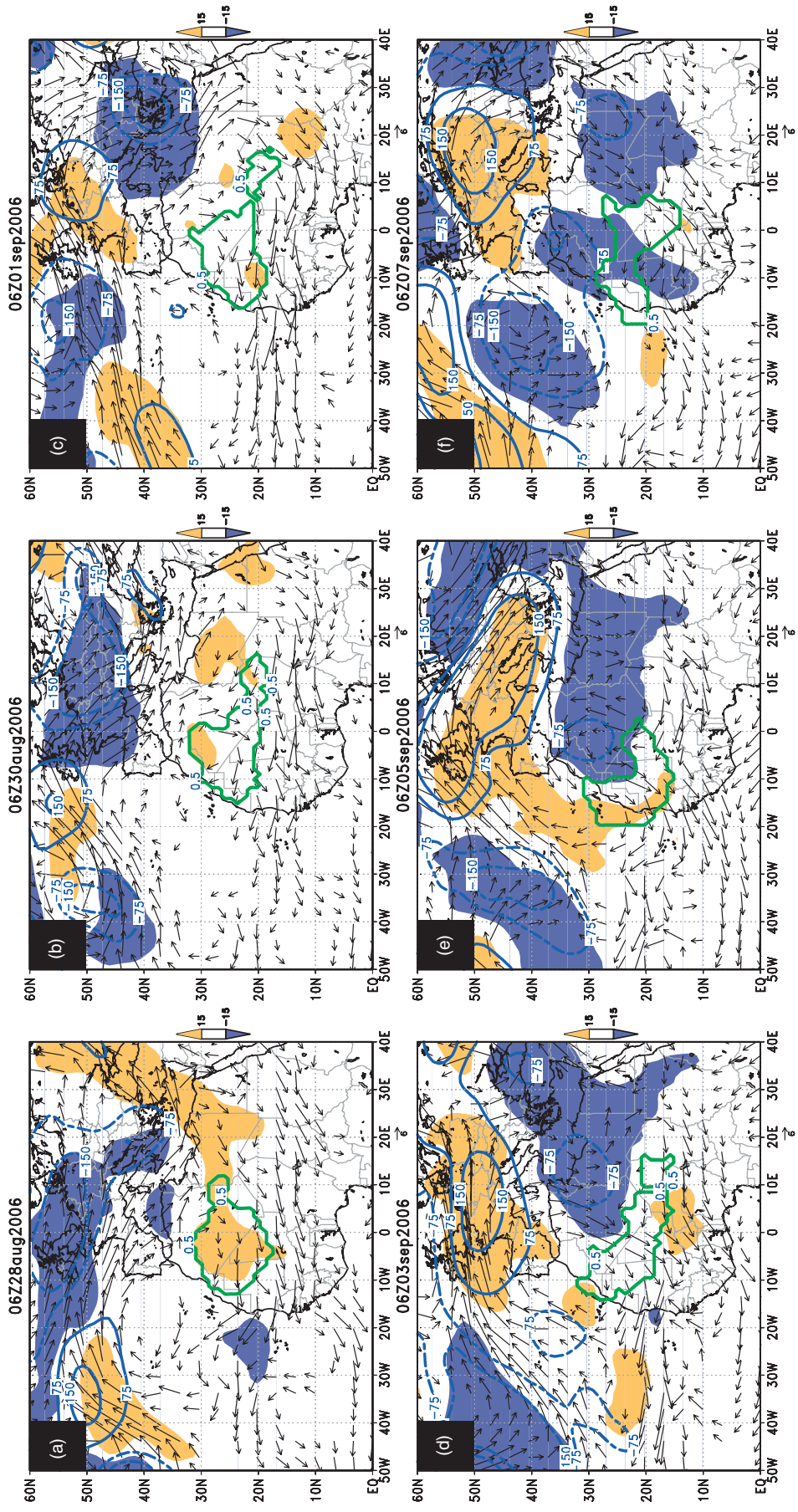

Figure 3. Anomaly of LLAT (m, dark shading negative, light shading positive), of the 700 hPa wind field ($m\,s^{-1}$, vectors) and anomaly of the 300 hPa geopotential height (−150, −75, +75 and +150 m contours) on (a) 28 August, (b) 30 August, (c) 1 September, (d) 3 September, (e) 5 September, and (f) 7 September 2006. The anomalies are computed independently for each grid box with respect to the average between 22 August and 7 September (one period of the 10–30 d pulsation). The location of the WAHL (solid contour) is also shown.

2(n) and (o). In spite of similarities with typical tropical plume events, this event does not fulfil the criteria defined by Fröhlich and Knippertz (2008) who use the mean potential vorticity between 400 and 100 hPa to detect the extratropical intrusions south to 25° and 17°N. The possible reason could be that these specific tropical plume events occur more often during the winter season. Thorncroft and Flocas (1997) have observed the same interaction between tropical and extratropical circulation, but the anomaly appear quite different and further to the south. This difference could be due to the distinct period of this study (during the winter season).

3.3. Investigation of the WAHL and wave activity variability in the 3–10 d period

Using the wavelet analysis of the meridional wind field at 700 hPa, we find significant signals associated with AEWs in the 3–5 and 6–9 d period band during the beginning of September. This is consistent with the results obtained for the year 2006 with the AEW detection method proposed by Berry *et al.* (2007) applied to National Centers for Environmental Prediction (NCEP) reanalyses (Janicot *et al.*, 2008).

To characterise the AEWs during this period, Figures 4 and 5 display the daily 700 hPa wind field at 0600 UTC filtered in the 3–5 d and the 6–9 d period bands, respectively, between 28 August and 7 September, when the waves were strongest.

On 28 August, the AEWs are located in the southern part of West Africa, over the Sudanian and Guinean regions (Figure 4(a)). The AEW activity increases over the Sahel thereafter. On 30 August, the day of the minimum of WAHL activity in the 3–10 d period, the ridge sector of an AEW is observed to be centred over the western edge of Mali, its northernmost part being located over the WAHL (Figure 4(b)). Between 1 and 3 September, the 700 hPa southerly sector of 3–5 d AEW is seen to penetrate the eastern part of the WAHL, whereas a strong northerly sector is distinguished over the western part of the WAHL. As shown by Fink and Reiner (2003) and Cuesta *et al.* (2009), southerly low-level winds associated with AEWs at 700 hPa (which is quite similar to the pattern of the filtered wind field at 850 hPa) could be associated with convective activity due to the increase of mean 925–700 hPa moisture advection from the Gulf of Guinea to the northern Sahel and southern Sahara. As a consequence, the decrease of temperature over the Sahel is consistent with the presence of the southerly wind of AEWs at 700 hPa seen in the 3–5 d filtered wind (Figure 4). This is a possible reason for the decrease of brightness temperature around 20°N, centred over the Hoggar on 31 August (Figure 2(h)), then over the southern part of Algeria on 1 September (Figure 2(i)), and finally over North Mauritania and Mali on 2 September (Figure 2(j)).

In spite of the impact of the AEWs on convection and temperature, this period of active convection over the Sahel (between 1 and 3 September) is associated with the strengthening period of the 3–10 d pulsation of the WAHL (dark bars in Figure 1(b)). The possible reason for this apparent contradiction could be due to the limited spatial extension of the impact of 3–5 d AEWs. In the 10.8 μm brightness temperature field, convection and/or cold advection reaches 22°N. Thus the northern part of the WAHL remains associated with high temperatures and thus the WAHL may indeed be strengthening north of 22°N. Thus the relationship between 3–5 d AEWs and WAHL pulsations appears limited on the southern part of the WAHL.

In Figure 5 we can observe the westward propagation of a 700 hPa trough and ridge of an 6–9 d AEW. These AEWs are located further north than the 3–5 d AEWs (i.e. over Algeria) and their wavelength is on the order of 4500 km in accordance with Diedhiou *et al.* (1998). On 3 September, during the maximum of the WAHL thickness of the 3–10 d pulsations (light bars in Figure 1(b)), the 6–9 d wave displays a northerly wind anomaly over the central Sahel (Figure 5(d)). On the contrary, days with minimum thickness of the WAHL are associated with a strong southerly wind (30 August and 7 September), especially on 7 September when the WAHL seems to be separated into two parts by this southerly flow (Figure 5(f)).

The collapsing of the WAHL seen in Figure 5(f) occurs with both the area of low 300 hPa geopotential height and a northeastward wind anomaly in the 700 hPa wind field (Figure 3(f)) and a southwesterly wind anomaly at 700 hPa which increases the advection of humid and cold air at low levels. This could illustrate the possible relationship between midlatitude circulations, defined here by the intrusion of low 300 hPa geopotential height, AEWs and WAHL pulsation. This interaction has already been proposed by Nicholson (1981).

To assess whether events such as the one described here are rare or occur regularly, we have studied these intraseasonal pulsations using climatological databases (ECMWF reanalyses and CLAUS).

4. Pulsations in the 10–30 d period band

4.1. Composite evolution

Between 1979 and 2001, the 10–30 d pulsation is distributed quite homogeneously through the rainy season. The preferred duration of these pulsations, defined as the period between two maxima of the WAHL thickness, was observed to be around 14 d (28% of cases). To obtain a coherent signal, associated with strong pulsations, and keep enough cases, only pulsations of filtered thickness with a maximum larger than ± 1.5 m are taken into account. This threshold selects 40% of total days in the summer season, when the WAHL is over the Sahara (LA09). Thus our composite is based on approximatively 3 or 4 pulsations per year. While not using any threshold or using different threshold values (± 2 m and ± 3 m), the same basic synoptic environment is generated as with ± 1.5 m, but with a decrease of the significance, or a decrease of the spatial pattern coherence due to the small

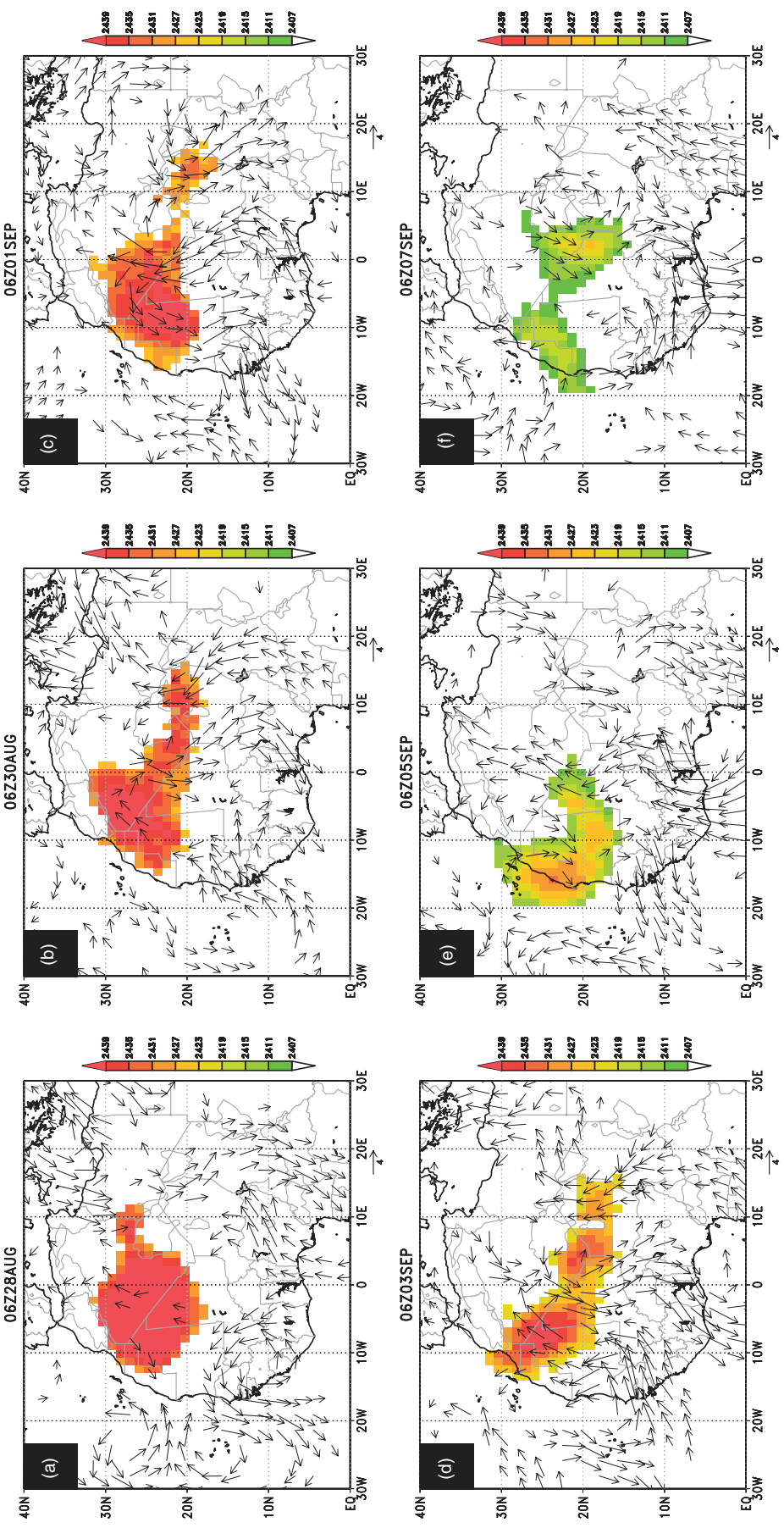

Figure 4. 3–5 d filtered wind at 700 hPa (m s^{-1}, vectors) and WAHL thickness (m, shading) on (a) 28 August, (b) 30 August, (c) 1 September, (d) 3 September, (e) 5 September, and (f) 7 September 2006.

number of events (1 event per year on average for the ±3 m threshold). The composite study performed uses the same methodology as Diedhiou *et al.* (2001) and decomposes WAHL pulsation in eight time steps. In our particular case, we select all pulsations with a periodicity between 10 and 30 d and with intensities larger than the chosen threshold. 70% of selected pulsations are between 13 and 16 d. Time step 1 (5) corresponds to the maximum (minimum) of the WAHL thickness filtered in the 10–30 d period band, thus to maximum (minimum) of the WAHL activity at this period band. Time steps 2-3-4 (6-7-8) represent the collapsing (strengthening) period of the WAHL. Due to the mirror structure of the composite study, where the maximum (collapsing) period is quite similar to the opposite pattern of the minimum (strengthening) period, we will focus on the peak WAHL and collapsing WAHL periods only. In Figure 6, we show the anomaly of the large-scale meteorological conditions as the difference between a given meteorological field at a given time step and the same field at the opposite time step.

During the maximum period of the WAHL (Figure 6(a)), the positive anomaly of LLAT is a maximum over the Sahel. At 700 hPa, just above the WAHL, the anomaly of the wind field during the maximum period with respect to the minimum period of the WAHL displays a wide anticyclonic circulation explained by the fact that, during high-thickness WAHL episodes, surface pressure decreases which favours the cyclonic circulation and convergence in the lower troposphere (Figure 8(a)) and divergence and anticyclonic circulation above the anomaly of temperature (LA09). This pattern exhibits several similarities with that evident on 28 August 2006, such as the anomaly of 300 hPa geopotential height over Morocco and Spain and the negative anomaly of the LLAT over Europe. Moreover, in spite of the fact that the anomaly appears weaker in 2006 than in the climatology, both figures describe the synoptic environment associated with positive anomaly of the WAHL.

During the first step of the collapsing period of the WAHL (Figure 6(b)), the positive anomaly of the LLAT moves northward located below a positive anomaly of geopotential height at 300 hPa over France. Using the composite of temperature at the same levels (not shown), we find a cold (warm) anomaly associated with the negative (positive) anomaly of the geopotential height. Thus, there is an upper-level wave over the Mediterranean with a cold trough in the eastern side and a warm ridge to the west. That causes a 700 hPa anticyclonic circulation with a surge of cold northeasterly wind from the Mediterranean to Libya (Figure 6(c)). On the eastern edge of the Mediterranean, the cold trough is displaced towards the south and reaches the Sahara. During the last time step of the collapsing period (Figure 6(d)), the Hoggar chain is underneath a 300 hPa cold trough. This trough affects the whole of the Sahara, and coincides with a negative anomaly in LLAT. As a consequence of the decrease of the WAHL activity, the 700 hPa wind field displays a cyclonic circulation over the Sahara. This evolution is consistent with the case-study in September 2006 (Figure 3).

These figures also allow us to describe the composite evolution of the AEJ, i.e. the large-scale easterly flow around 700 and 600 hPa over the West Africa (between 5 and 15°N). During the maximum period of the WAHL, the anticyclonic circulation over the Sahel leads to the strengthening of the AEJ west of 10°E (Figure 6(a)). Then, during the three steps of the collapsing period, the AEJ intensity starts to decrease in intensity, initially over the eastern Sahel (Figure 6(b)), then over the central Sahel (Figure 6(c)) and finally over the whole of the Sahel (Figure 6(d)) as demonstrated by the negative wind anomaly.

In conclusion, we have identified the impact of the upper-level trough which penetrates from the Mediterranean into the north of West Africa and which modulates the WAHL intensity and location in the 10–30 d period. This composite evolution looks like the surges of cold air from the Mediterranean into the northern part of Africa during the boreal summer presented by Vizy and Cook (2009). These authors identify a similar northerly wind from the Mediterranean but with a higher occurrence frequency than in the present study (more than 6–10 cases per year). In spite of the use of different methodologies, we observe also a similar eastward then southward propagation of the cold upper-level front. Moreover, Chauvin *et al.* (2009) have also highlighted the influence of mid-latitude circulations on the 850 hPa temperature field in the northern part of the Sahara. Chauvin *et al.* (2009) have also shown the east–west displacement of the location of the maximum temperature field. This is consistent with our result showing the westward propagation of the anomaly of the WAHL location from a position west of the Hoggar during the strengthening period of the WAHL intensity to a more western position during the collapsing period of the WAHL activity (Figure 7(a)).

4.2. Link with convection

The maximum thickness of the WAHL is associated with wide positive anomaly of convective activity east to 10°E (Figure 8(a)), whereas the western side of the Sahel is associated with a significant decrease of convection in the northerly anomaly in the 925 hPa wind field. During the three steps of the collapsing period (Figures 8(b), (c), (d)), we observe the westward displacement of the positive anomaly of the convective index from Sudan to Mali. Convection favours the migration of humid and cold air masses toward the west of the WAHL due to the associated decrease of the surface temperature related to cloud cover and the increase of the surface humidity linked with rainfall. Near the Guinea coast, the convective activity decreases during this period, and we note a north–south dipole of convection between the latitude of the Sahel (around 18°N) and the Guinean coast (around 5°N). This evolution of the convective activity occurs without a significant evolution of the wind field south to 15°N, whereas over Libya the penetration of the cold depression is seen to be associated with a strong northeasterly 925 hPa wind. Note that during the collap-

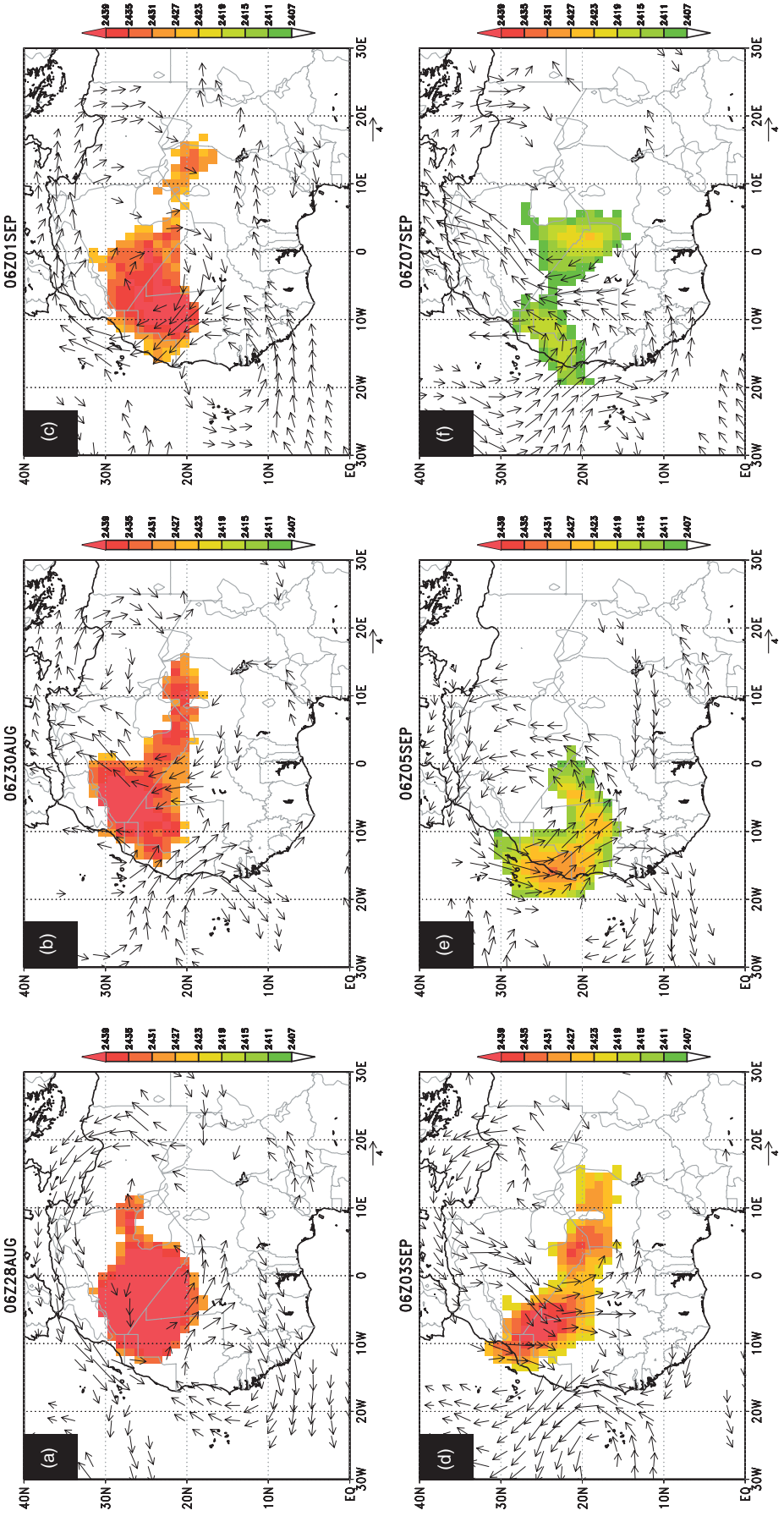

Figure 5. As Figure 4, but showing 6–9 d filtered wind at 700 hPa ($m\,s^{-1}$, vectors) and WAHL thickness (m, shading).

sing period, the 700 hPa wind field displays a westward propagating negative anomaly between 5° and 15°N (Figures 6(c), (d)). This depicts a decrease of the AEJ during the increase of the convective activity over the Sahel. This result is in accordance with the dynamical environment of the wet period of the monsoon flow discussed by Sultan *et al.* (2003) and Lavaysse *et al.* (2006). When the activity of the WAHL is weak, the wind direction changes over Mauritania, from southward to northwestward. In the low troposphere, between 925 and 700 hPa, humidity and temperature advections do not exhibit a coherent signal, thereby suggesting that this pulsation could be generated by the penetration of an upper-level trough from the midlatitudes over West Africa.

These results are in accordance with the study of Chauvin *et al.* (2009), with two small differences. These authors highlighted the decrease of outgoing long-wave radiation over Chad and Sudan concomitantly with the maximum period of the heat low, whereas here the maximum occurs more during the collapsing period. In their study the anomaly of convection moves westward with the same propagation characteristics as AEWs. In our study, the displacement of the convection anomaly appears to be slower than that of the AEWs.

5. Pulsations in the 3–10 d period band

5.1. Description of synoptic environment

In ERA-40 reanalyses, both the number and the intensity of 3–10 d pulsations are slightly larger in July and August than during the rest of the season. The most frequently detected time separation between two maxima is found in the 5–7 d range (respectively 30% and 33% of total number of pulsations for July and August). We used a threshold of ±2 m on filtered WAHL thickness to select the same number of days as in the case of the 10–30 d period band (around 40% of the total number of cases). Only two steps are shown for the maximum and collapsing period of the WAHL (Figure 9).

During the maximum intensity of the WAHL (Figure 9(a)), an anticyclonic circulation is detected, centred approximately at 26°N, 20°W. This circulation induces a wide northerly anomaly of the 700 hPa wind field over the Sahel which comes from the Mediterranean. Two areas of positive anomaly of LLAT can be distinguished during this period (Figure 9(a)) which indicate a strengthening of the WAHL. The first positive anomaly is centred over the anticyclonic circulation of the 700 hPa wind field. The second and largest anomaly is centred in the northerly wind area over the Mauritanian/Mali border. These large-scale circulations and the anomaly of LLAT seem to be linked with the anomaly of the 300 hPa geopotential height (contours in Figure 9(a)) and the midlatitude circulation. Indeed, over the British Isles, the positive anomaly of 300 hPa geopotential height and the 700 hPa wind circulation suggest the presence of a ridge. This interaction between the ridge in midlatitudes with the ridge centred over the Mauritania coast could favour the southward (northward) advection of warm (cold) air at 700 hPa over the Sahara during the period of maximum (minimum) WAHL activity. In response to these anomalies, the location of the WAHL is more often detected over the western Sahara (around 5°W, positive anomaly in Figure 7(b)) where the northerly wind induces an increase in the advection of the dry and warm air (Figure 10(a)). At the same time, the WAHL is less often located in the eastern part of West Africa (over Niger and Algeria) in comparison with the mean summer season location. Then, during the collapsing period (Figure 9(b)), the anomalies of wind and LLAT have moved westward in agreement with the propagation of AEWs, whereas over Europe the anomaly of the 300 hPa geopotential height propagates eastward. Due to the fluctuation of the time lag between the maximum and the minimum period of the WAHL (between 2 and 5 d), it is more difficult to clearly identify the speed of the westward propagation from these wind fields. They can be in agreement with the propagation speed of either 3–5 d AEWs or 6–9 d AEWs. The centre of cyclonic circulation is now located over Algeria (30°N, 0°E). The positive anomaly of LLAT located over the anticyclonic circulation has the same intensity, whereas the second maximum, located over the northerly wind anomaly, decreases with respect to the previous time step (i.e. Figure 9(a)). The proximity of this latter area to the Atlantic could limit the dry and warm advections towards the WAHL and thus limit the amplitude of the LLAT anomaly. Along the eastern edge of the trough (east of 5°E), a wide southerly anomaly of wind field appears. Advection of cold and humid air (Figure 10(b)) occurs in an area of negative anomaly of LLAT in the southern part of Niger and over Algeria which contributes to decrease the WAHL detection over the eastern part of Sahel and could be associated with the westward propagation of this negative anomaly in Figure 7(b). During the period of minimum WAHL thickness, we find that the negative LLAT anomaly corresponds to the merging of two anomalies. The first corresponds to the westward propagation of the low pressure ridge detected over Niger during the collapsing period. The second anomaly is located further north, over Algeria and Tunisia.

While the AEJ is stronger at the time when the WAHL activity is a maximum in the 10–30 d period, the AEJ intensity exhibits a marked east–west dipole during the time the WAHL activity is a maximum in the 3–10 d period. We note a slight increase of the AEJ intensity over Senegal and the West African coast, and a slightly decrease over the Sahel. This decrease is more pronounced during the collapsing period over the Sahel.

In conclusion, we find a second possible interaction between the WAHL and the midlatitude circulation. The ridge (trough) circulation which propagates westward over the Tropics merges with another ridge (trough) over midlatitudes which propagates eastward. This interaction could explain the large-scale anticyclonic (cyclonic) circulation with large warm and dry (cold and wet) advections over the Sahara from the north (south) and thus the increase (decrease) of the WAHL activity.

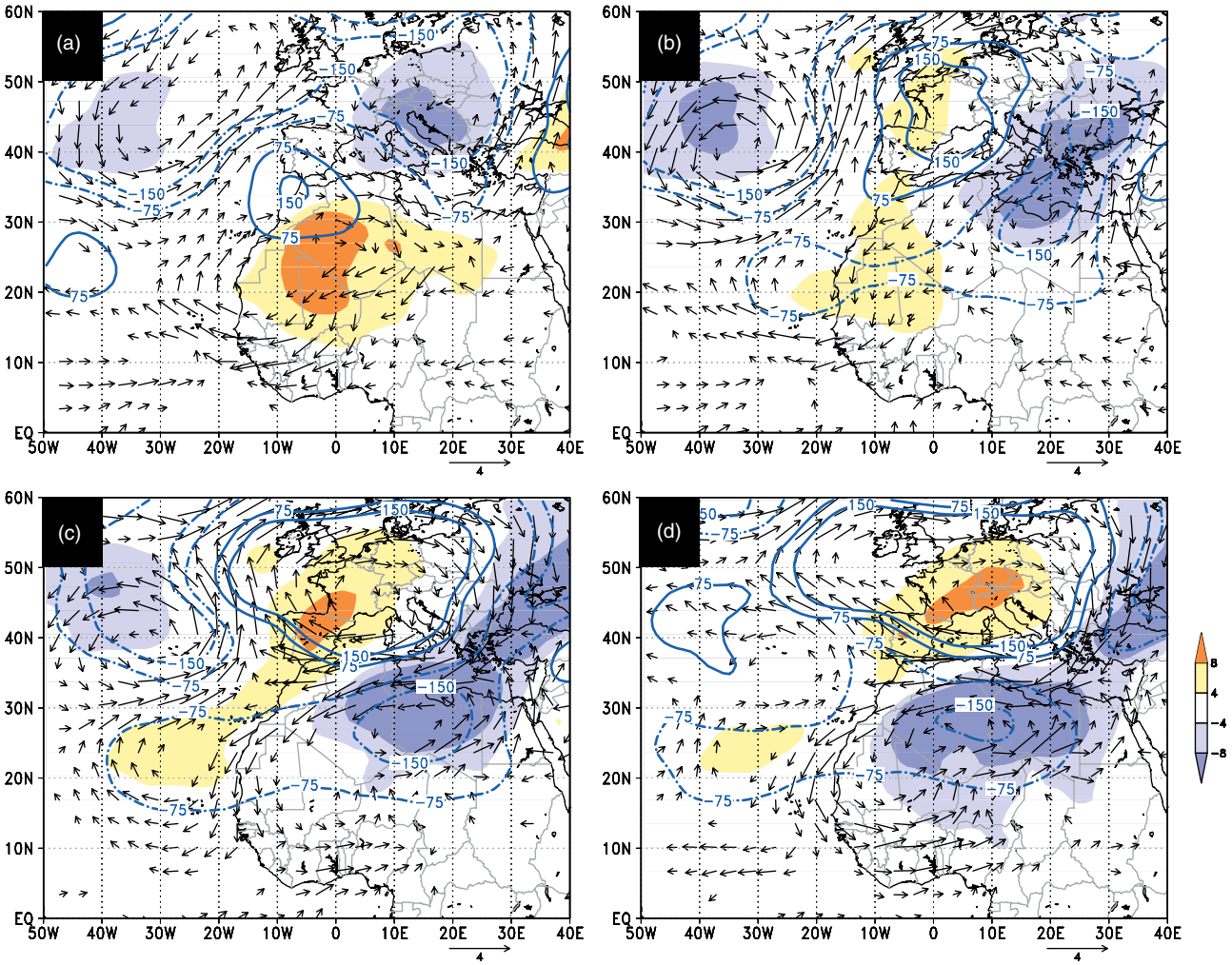

Figure 6. Composite analysis in the 10–30 d period band of the anomaly of LLAT (m, shading), of the 300 hPa geopotential height (−150, −75, +75 and +150 m contours) and of the 700 hPa wind field (m s^{-1}, vectors). The anomaly shown in (a) is computed as the difference between the time of maximum WAHL activity and the time of minimum WAHL activity. Similarly, (b), (c) and (d) represent the anomaly fields at three stages of the collapsing WAHL phase and are computed with respect to three stages of the strengthening WAHL phase.

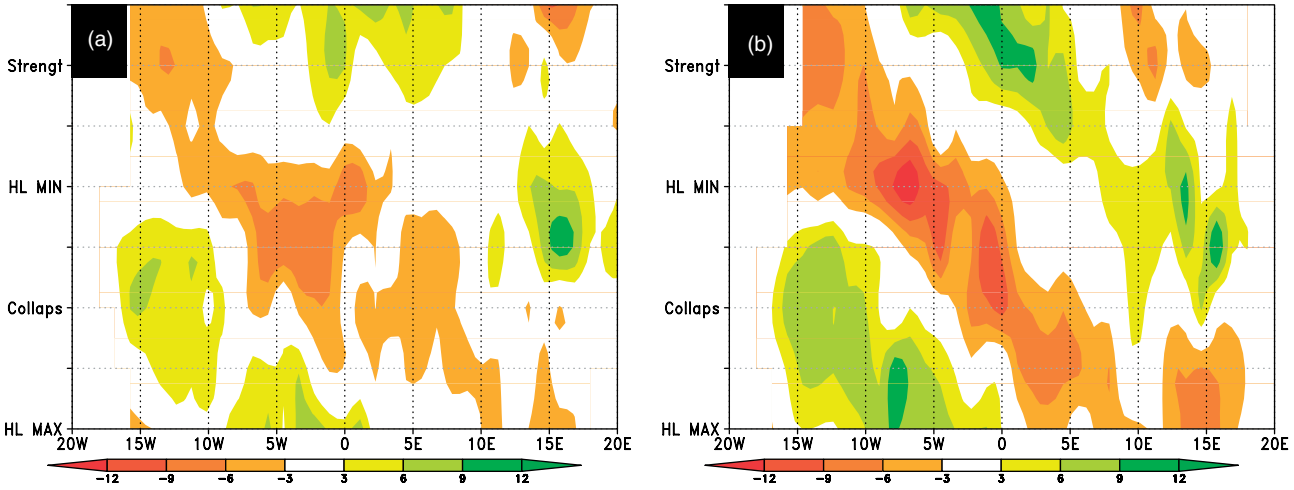

Figure 7. Longitudinal and temporal anomaly of the mean WAHL location (in %) in relation to the mean summer location, for (a) the 10–30 d period pulsations, and (b) for the 3–10 d period pulsations of the WAHL.

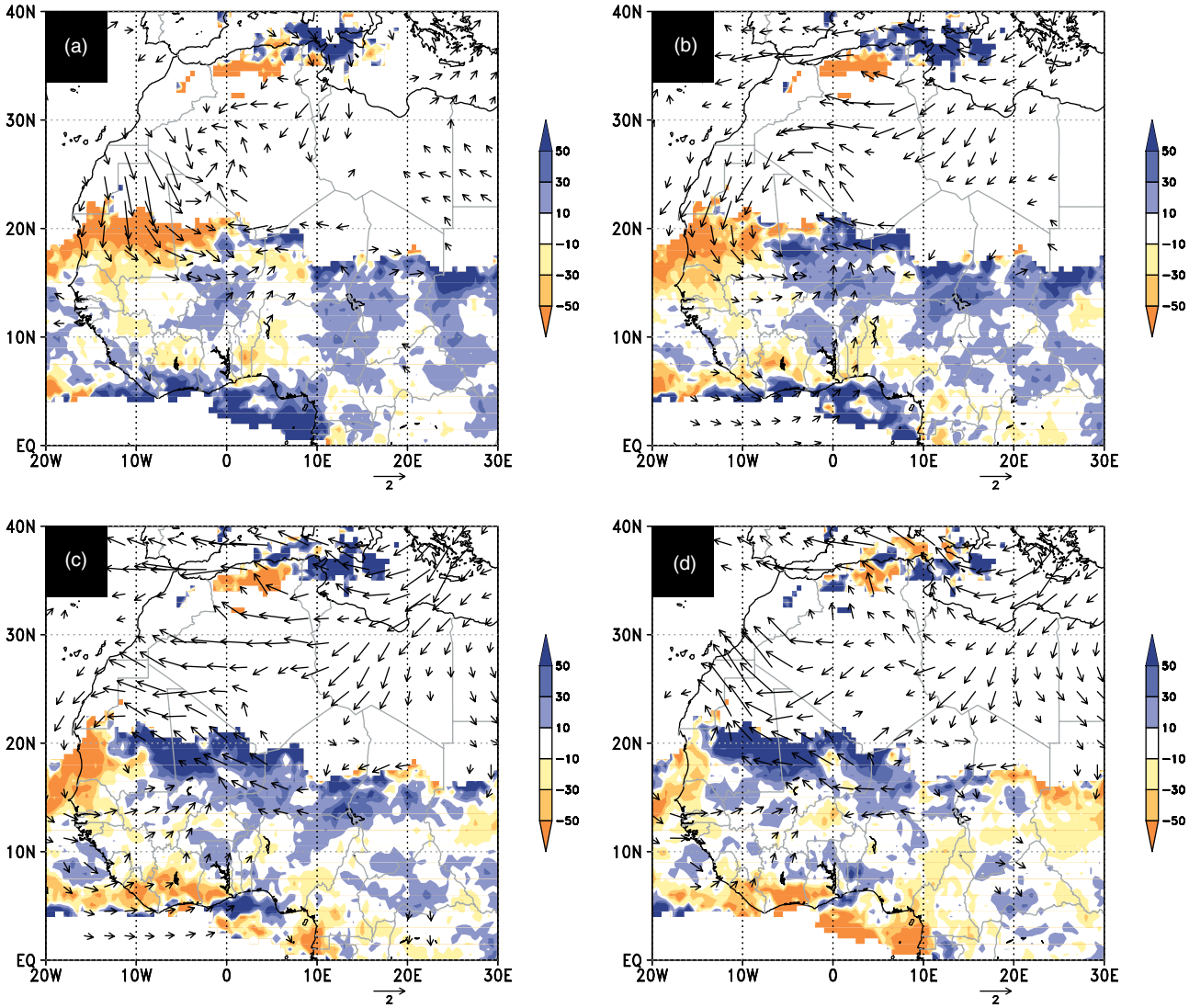

Figure 8. As Figure 6, but for the convective index computed from CLAUS (%, shading), and the 925 hPa wind field (m s^{-1}, vectors).

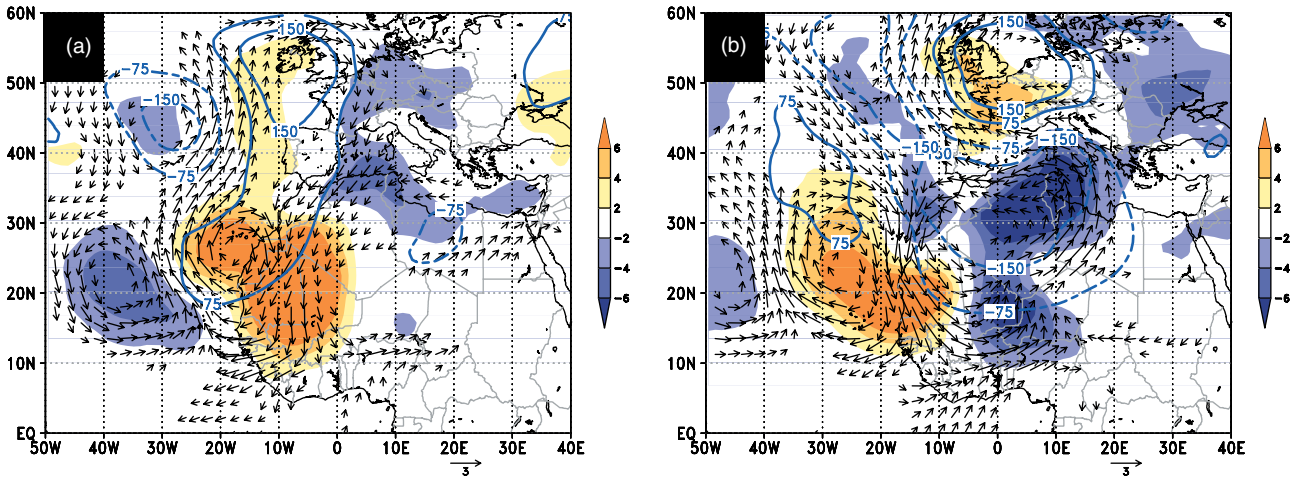

Figure 9. Composite analysis in the 3–10 d period band of the anomaly of LLAT (m, shading), of the 300 hPa geopotential height (m, −150, −75, +75 and +150 m contours) and of the 700 hPa wind field (m s^{-1}, vectors). The anomaly shown in (a) is computed as the difference the time of maximum WAHL activity and the time of minimum WAHL activity. Similarly, (b) represents the anomaly fields at one stage of the collapsing WAHL phase, computed with respect the opposite stage of the strengthening WAHL phase.

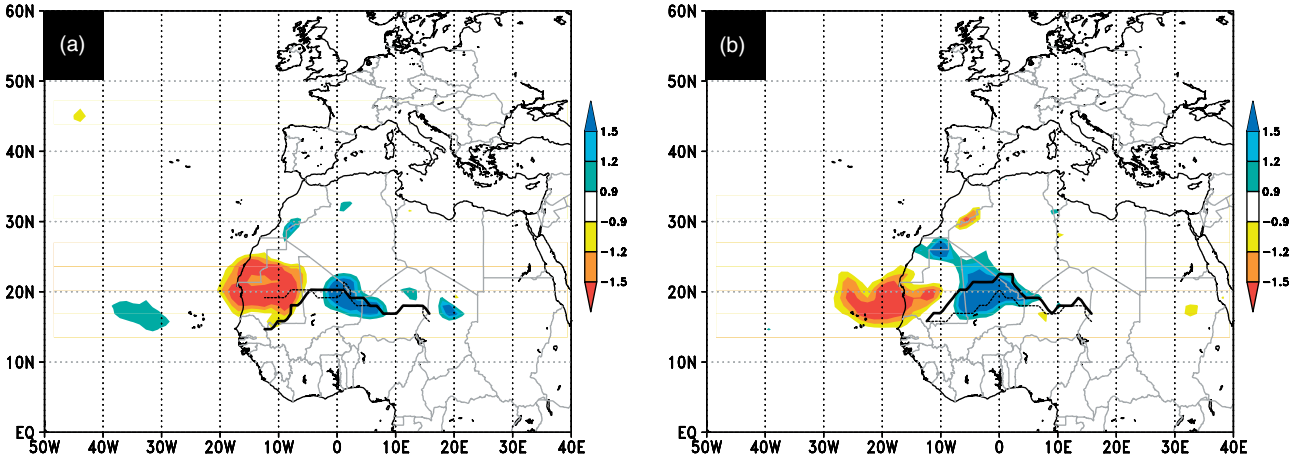

Figure 10. As Figure 9, but for moisture advection ($g\,kg^{-1}\,d^{-1}$) averaged between 925 and 700 hPa. The thick solid (thin dotted) line displays the location of the ITD during (a) the period of maximum (minimum) WAHL activity and (b) the period of collapsing (strengthening) period of the WAHL. The position of the ITD is determined as the boundary delineating the region where both the meridional and the zonal winds are positive.

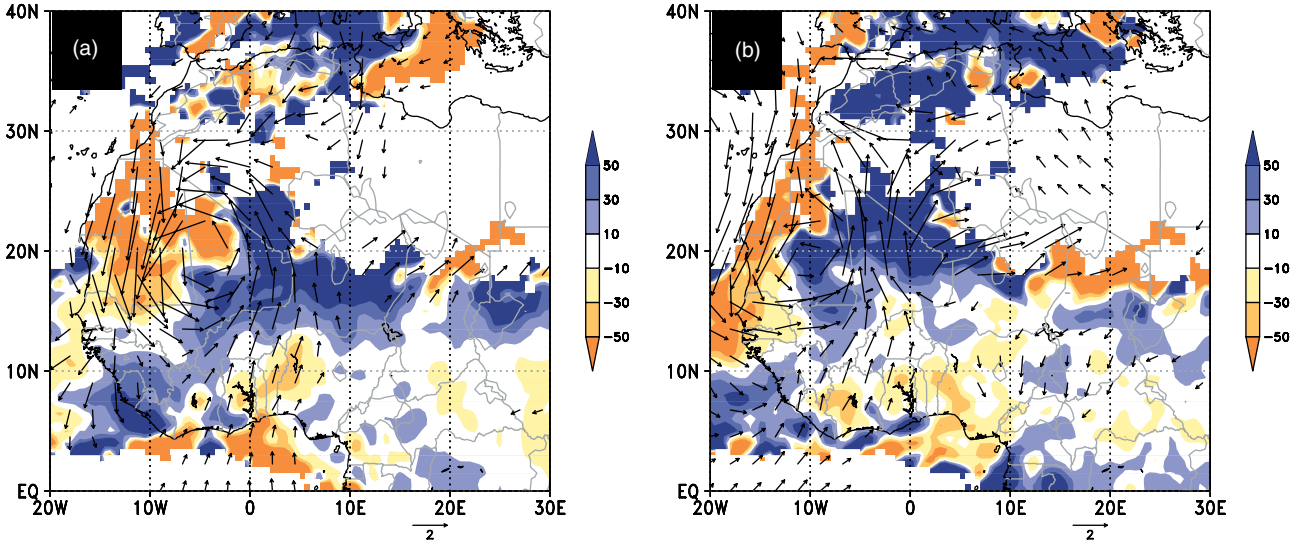

Figure 11. As Figure 9, but for the wind field at 925 hPa ($m\,s^{-1}$, vectors) and the convective index from CLAUS brightness temperature anomaly (shading, %).

5.2. Link with convection

During the maximum activity of WAHL (Figure 11(a)), the wind field at 925 hPa describes the wide cyclonic circulation over West Africa centred at the increase of the WAHL detection (5°W, 20°N). As a consequence, a significant warm advection (Figure 10(a)) associated with the northeasterly 925 hPa wind field generates a negative anomaly of convection over Mauritania. In the southerly wind (east of 5°E), in agreement with the increase of cold and humid advections from the south, a large positive anomaly of convection is obtained over the whole of the central Sahel (between 5°W and 10°E as well as between 10 and 15°N). During the collapsing period (Figure 11(b)), the maximum of surface temperature and the WAHL location have moved westward in accordance with the warm advection on the west side of the WAHL and the cold advection to the east. The southerly wind reinforces the convection which extends over the Sahel and the Saharan areas. At the same time, we note a decrease of the AEJ intensity over the Sahel. This anomaly corresponds to the northernmost location of the convection. Moreover, the location of the ITD displays a significant northward migration compared with the strengthening period (Figure 10(b)). This influence of the WAHL on the ITD location during the rainy season over the Sahel could be compared with the pulsation of the ITD in the 3–5 d period shown by Couvreux *et al.* (2009) during the pre-monsoon season.

5.3. Relationship with AEWs

The sequence of alternating cyclonic and anticyclonic circulation anomalies in the 700 hPa wind field which propagate westward is reminiscent of another synoptic component of the West African monsoon, namely the AEWs. Several characteristics are in agreement with the 3–5 d AEWs. As we have shown earlier, one of the most

frequently detected time separations between two maxima of the 3–10 d pulsation of the WAHL is around 5 to 7 d (more than 30% of total number of pulsations). Thus, in this part, we discuss the possible role of the 3–5 d AEWs and 6–9 d AEWs in the 3–10 d period band of the WAHL pulsations.

5.3.1. 3–5 d AEWs

To describe the impact of the mean wind associated with each sector of the wave (namely northerly, trough, southerly and ridge sectors) on the LLAT, we perform a composite study. We have used a methodology inspired by the study of Diedhiou *et al.* (2001) in which the 3–5 d AEWs are detected when the intensity of the 3–5 d filtered meridional wind at 700 hPa averaged in the area (8°W–2°E; 15°N–25°N) is larger than 1.5 m s^{-1}. This area is chosen for two reasons: first, it corresponds to the area of the largest wind field anomaly in the 3–10 d WAHL pulsation analysis (Figures 9) and, second, it is located in the preferential trajectory of the AEWs. Maxima (minima) of the meridional filtered wind field determine the southerly (northerly) sector. Transition regions between maxima and minima (minima and maxima) are defined as ridge (trough) sectors.

The 700 hPa level is appropriate to detect the 3–5 d AEWs over the Sahel. Indeed, in the northern part of the AEJ region, the waves are generally best detected between 925 and 850 hPa, while in the southern part of the AEJ they are generally best detected at 700 hPa (e.g. Janicot *et al.*, 2008) using NCEP reanalyses. However, in this study, the 3–5 d AEWs to the north are best detected at 700 hPa in the ECMWF reanalysis.

Using Figures 9 and 12, it is possible to compare the structure of the anomaly fields of the 3–5 d AEWs and of 3–10 d WAHL pulsations.

The spatial correlation between the WAHL pulsation anomaly pattern and the 3–5 d AEW anomaly pattern is highest when an AEW trough is positioned over the WAHL region during a period of maximum intensity of the WAHL (spatial correlation of 0.48 for the LLAT and of 0.44 for the wind field). Nevertheless, we can observe some differences between these patterns in Figure 12. The anomaly of the 700 hPa wind field during the trough sector (computed as the difference between the composite wind fields associated with the trough and ridge sectors of the wave), displays a cyclonic circulation over West Africa centred on the Algeria/Mali border. This result is in agreement with the methodology used to detect the waves. This circulation is associated with an increase of the LLAT (+5 m) in the region of northerly wind. In comparison with the period of maximum WAHL activity (Figure 9(a)), the location of the northerly wind is close to that seen during the period of the trough (Figure 12(a)), but the wavelength and the size of the cyclonic circulation are larger in the WAHL composite than in the 3–5 d wave composite. More generally, the 3–5 d AEWs show a local signature in the wind field and in the LLAT anomalies around the detection box and no significant signal north of 30°N, whereas the WAHL composite displays a more widespread impact with a significant wind signal over the northern part of West Africa. The comparison of the large-scale wind field anomaly in the southerly wind sector of the 3–5 d AEWs with the anomaly in the collapsing period of the 3–10 d pulsations of the WAHL reveals several discrepancies. The extensions of LLAT and wind field anomalies are larger in the WAHL than in AEW composites. AEWs impact only a small band of LLAT (around 10 to 30°N), whereas the WAHL composite is associated with significant signals in wind and LLAT anomalies over the Mediterranean and Europe.

In conclusion, the present analysis suggests that the 3–5 d AEWs interact with the southern edge of the WAHL (e.g. Figure 12). On the other hand, in order to penetrate deeply into the WAHL and affect the 3–10 d pulsations of the WAHL, 3–5 d AEWs would need to be enhanced through interactions with the midlatitude perturbations, which generate a coherent signal north to 30°N, as shown in Figure 9.

5.3.2. 6–9 d waves

The spatial correlation over the area shown in Figures 13 between the composite of the 6–9 d waves and the 3–10 d WAHL pulsations is the largest when the maximum period of the WAHL is simultaneous with the northerly sector of the 6–9 waves (spatial correlation of 0.73 for the LLAT, and around 0.75 for the wind field at 700 hPa). In the north sector (Figure 13(a)), the cyclonic circulation over Algeria is more widespread and located more to the north (around 25°N) than in the 3–5 d AEW composite. The location of the positive anomaly of LLAT is coherent with both the northerly wind over Mali and Mauritania and with the anticyclonic circulation over the Atlantic Ocean (20°W, 30°N), close to the coast, as shown in the WAHL pulsation. Over the Mediterranean, a wide negative anomaly of LLAT is observed which could be associated with the displacement or the intensification of the Libyan anticyclone. The anomaly of thickness and of the wind field are more coherent with the composite of WAHL pulsations than to the composite of AEWs, nevertheless the 300 hPa geopotential anomaly shows some discrepancies. The latitudinal extension of the anomaly is much weaker than in the WAHL composite and thus we observe very low interactions between the midlatitudes and these waves. The two negative anomalies, over the Mediterranean and Niger, propagate westward in the trough sector (Figure 13(b)). During this period, the negative anomaly of LLAT over Niger increases and is located in the southerly anomaly of the 700 hPa wind field. West of the Sahel (15°W) the positive anomaly of LLAT located over the continent reaches the Atlantic coast and starts to decrease. This is in agreement with the collapsing period of the WAHL (Figure 9(b)).

In conclusion, the 6–9 d wave composite has a strong and widespread signature in the northern part of the Sahel. We find some agreements with the WAHL composite, and more than 60% of 3–10 d WAHL pulsations occur during significant 6–9 d wave pulsations. Nevertheless, in the 6–9 d waves, we do not find the same pattern

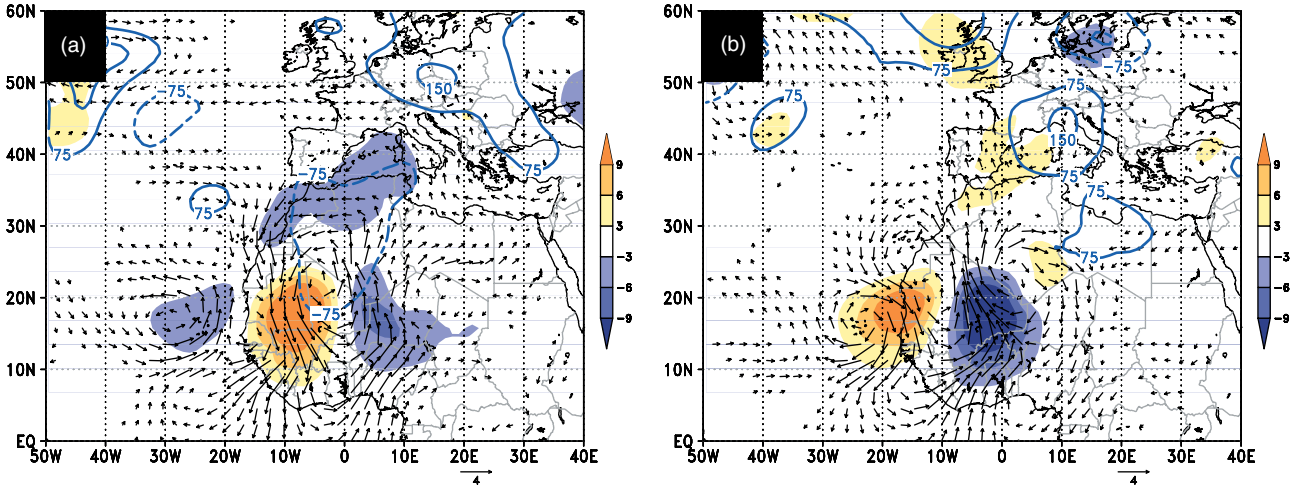

Figure 12. Composite study of the 3–5 d AEWs shown in terms of anomaly between (a) the trough sector minus the ridge sector and between (b) the southerly sector minus the northerly sector. The composite analysis in the 3–10 d period band of the wind field at 700 hPa ($m\,s^{-1}$, vectors), the LLAT anomaly (m, shading) and the 300 hPa geopotential height anomaly contours (−150, −75, +75 and +150 m) are shown.

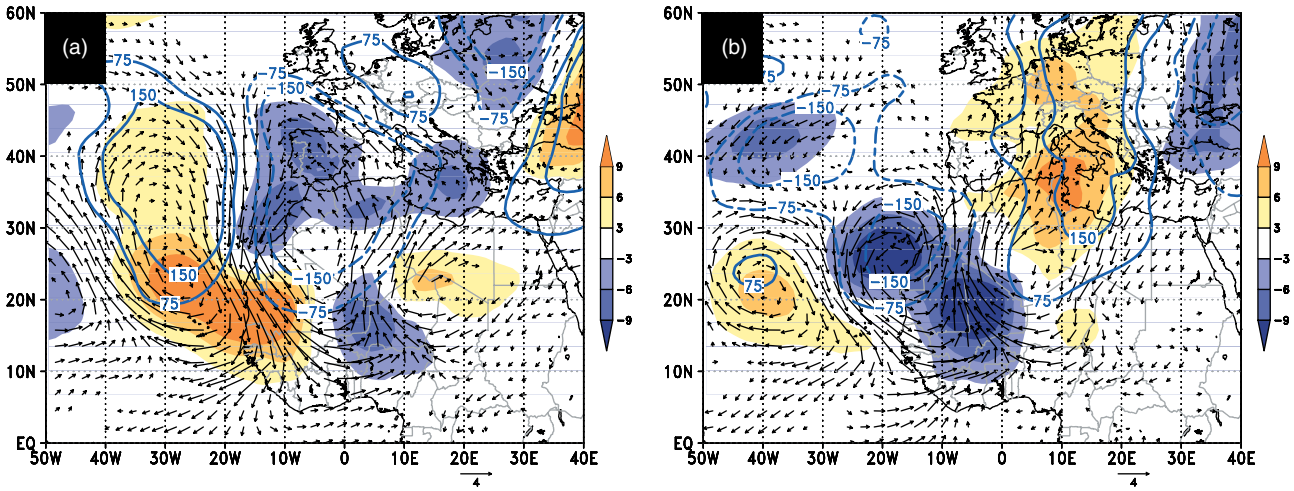

Figure 13. As Figure 12, but showing the composite study of 6–9 d waves.

of the 300 hPa anomaly of geopotential height and the geopotential anomaly displaces only westward, whereas in the 3–10 d WAHL composite, the northern part displaces eastward. Moreover, in this study, it is not possible to know the origin of the 6–9 d waves. They could be directly associated with WAHL pulsations, or associated with a pulsation of the Libyan anticyclone.

6. Conclusion

The WAHL –also called the Saharan Heat Low during the summer season –is a key element of the West African monsoon system, especially between June to September. In this study we propose to extend the study of the seasonal cycle of the WAHL (LA09) to intraseasonal time-scales. The intraseasonal variability of the WAHL is characterised using the LLAT variable defined by LA09. A case-study from the AMMA SOP in 2006 is used to illustrate the WAHL variability at intraseasonal scales. The WAHL exhibited pulsations at different time-scales during the summer of 2006 and collapsed at the beginning of September concomitantly with the largest convective event observed over the Sahara during the summer. Using wavelet analysis of the LLAT time series in the summer of 2006, we identify two significant period bands of pulsations of the WAHL: the first at 3–10 d and the second at 10–30 d. A similar wavelet analysis was conducted on LLAT time series in the summer using the ECMWF ERA-40 reanalysis between 1979 and 2001. The same 3–10 d and 10–30 d WAHL pulsation periods were detected, thereby proving the 2006 signal to be robust and representative at the climatological scale. To assess the dynamical environment associated with such events and their links with convection at the climatological time-scale, we have performed a composite study of these cases using the 3–10 d and 10–30 d filtered band of the LLAT.

In the ECMWF-based composite study, the collapsing phases of the WAHL in the 10–30 d period band appear to have an extratropical origin, in the form of an upper-level wave over the Mediterranean (detected at 700 hPa) with a warm ridge in the west and a cold trough in the

east causing the surge of cold air from Libya into the Sahara. As in Chauvin *et al.* (2009), we find westward propagation of the upper-level trough which penetrates over West Africa. These events are associated with strong negative temperature anomalies which favour the collapsing of the WAHL. Such penetrations of relative cold air were also studied by Vizy and Cook (2009) and have been shown to have a strong impact on the monsoon system circulation. In the present study, we have unambiguously highlighted the relationship between these midlatitude circulations and the WAHL as well as with the convective activity over West Africa. Such events are responsible for the negative anomaly of LLAT mostly observed along the northern side of the WAHL. The link between these WAHL pulsations and the modulation of the AEJ illustrated in the composite study could be important due to the relationship between the AEJ and the AEWs studied by Leroux and Hall (2009). Indeed, the period of maximum WAHL which is associated with strong AEJ could be a favourable environment to develop strong AEWs.

The composite analysis also revealed the WAHL variability in the 3–10 d band to be most important over West Africa and particularly in the ITD region. This variability can be explained by the westward propagation of cyclonic and anticyclonic circulation centres at 700 hPa (possibly 3–5 d AEWs or 6–9 d waves). It has been showed that during collapsing periods of the WAHL, the northward displacement of the southerly monsoon flow increased advection of cold and humid air. This advection tends to decrease temperature in the low troposphere over the Sahara and thus decrease the WAHL activity. The weakening of the WAHL is consistent with an increase of convective activity during this period over the Sahel, as derived from the satellite-based CLAUS long-term database. The possible link between WAHL variability at these scales and travelling 3–5 d AEWs and 6–9 d waves are discussed also. The signature of the travelling AEWs is found not to be sufficient to explain the composite pattern of 3–10 d pulsations of the WAHL. The 6–9 d waves travelling across West Africa generate a wider signature over the Sahel and appear to be a better link with the composite study of the 3–10 d WAHL pulsations.

Regarding the 2006 case-study, the large decrease of WAHL activity between 30 August and 7 September can be influenced by both westward travelling waves and extratropical circulation. A southerly wind associated with the 6–9 d waves contributes to the collapse of the southern edge of the WAHL on 30 August and 7 September via the enhancement of moist and cold advections. This advection also favours the development of widespread convective systems as observed with SEVIRI during this period. The most detrimental conditions to the maintenance of a strong WAHL occur on 5 September and are concomitant with the extratropical intrusion from Europe. A wide cold upper-level trough over the Mediterranean propagates southward and generates the surge of a cold air mass from the Mediterranean into the Sahel. This cold air surge tends to displace the WAHL to the south and west. On 5 and 7 September, the low-level southerly winds associated with the southerly sectors of both 3–5 d and 6–9 d AEWs are responsible for the transport of moisture into the WAHL region from the south. SEVIRI imagery reveals the presence of widespread convection on the north and south sides of the WAHL, associated with these humidity advections. On 6 September, the two convective cells merge to form a large southwest to northeast oriented band of convection which resembles a tropical plume event but does not satisfy the criteria defined by Knippertz (2005). The WAHL is shallowest on this day and the following one (7 September).

The impact of the intraseasonal variability of the WAHL on the low-level circulation and on convection is particularly significant over the Sahel. This study identifies synoptic components which could be associated with significant pulsations of the WAHL at intraseasonal scales. We have shown that extratropical intrusions are concomitant with strong modulations of the WAHL. Further analyses are currently being conducted to investigate the links between the WAHL variability at intraseasonal time-scales and the intraseasonal variability of the rainfall over West Africa, and over the Sahel in particular.

Acknowledgements

Based on a French initiative, AMMA was built by an international scientific group and is currently funded by a large number of agencies, especially from France, UK, USA and Africa. It has been the beneficiary of a major financial contribution from the European Community's Sixth Framework Research Programme. Detailed information on scientific coordination and funding is available on the AMMA International web site http://www.amma-international.org.

References

Berry G, Thorncroft C, Hewson T. 2007. African easterly waves during 2004 – Analysis using objective techniques. *Mon. Weather Rev.* **135**: 1251–1267.

Brest CL, Rossow WB, Roitier MD. 1997. Update of radiance calibrations for ISCCP. *J. Atmos. Oceanic Technol.* **14**: 1091–1109.

Burpee RW. 1972. The origin and structure of easterly waves in the lower troposphere in North Africa. *J. Atmos. Sci.* **29**: 77–80.

Chauvin F, Roehrig R, Lafore J-P. 2009. Intraseasonal variability of the Saharan heat low and its link with midlatitudes. *J. Clim.* submitted.

Couvreux F, Guichard F, Bock O, Campistron B, Lafore J-P, Redelseperger J-L. 2009. Synoptic variability of the monsoon flux over West Africa prior to the onset. *Q. J. R. Meteorol. Soc.* **136**(s1): 160–174.

Cuesta J, Lavaysse C, Flamant C, Mimouni M, Knippertz P. 2009. Nortward burst of the West African monsoon and interactions with large-scale conditions leading to rainfall over the Hoggar Massif, Algeria *Q. J. R. Meteorol. Soc.* **136**(s1): 175–190.

Diedhiou A, Janicot S, Viltard A, de Félice P. 1998. Evidence of two regimes of easterly waves over West Africa and the tropical Atlantic. *Geophys. Res. Lett.* **25**: 2805–2808.

Diedhiou A, Janicot S, Viltard A, de Félice P, Laurent H. 1999. Easterly waves regimes and associated convection over West Africa and the Tropical Atlantic: Results from the NCEP–NCAR and ECMWF reanalyses. *Clim. Dyn.* **15**: 795–822.

Diedhiou A, Janicot S, Viltard A, de Félice P. 2001. Composite patterns of easterly waves disturbances over West Africa and the tropical Atlantic: A climatology from the 1979–95 NCEP–NCAR reanalysis. *Clim. Dyn.* **18**: 241–253.

Duvel JP. 1990. Convection over Tropical Africa and the Atlantic ocean during northern summer. Part II: Modulation by Easterly Waves. *Mon. Weather Rev.* **118**: 1855–1868.
Fink A, Knippertz P. 2003. An extreme precipitation event in southern Morocco in spring 2002 and some hydrological implications. *Weather* **58**: 377–392.
Fink AH, Reiner A. 2003. Spatio-temporal variability of the relation between African easterly waves and West African squall lines in 1998 and 1999. *J. Geophys. Res.* **108**.
Fröhlich L, Knippertz P. 2008. Identification and global climatology of upper-level troughs at low latitudes. *Meteorol. Zeitschrift* **17**: 565–574.
Fu R, Del Genio A, Rossow WB. 1990. Behavior of deep convective clouds in the tropical Pacific from ISCCP radiances. *J. Climate* **3**: 1129–1152.
Hanstrum BN, Wilson KJ, Barrell SL. 1990. Prefrontal troughs over southern Australia. Part I: A climatology. *Weather and Forecasting* **5**: 22–31.
Janicot S, Ali A, Ascencio N, Berry G, Bock O, Bourles B, Caniaux G, Chauvin F, Deme A, Kergoat L, Lafore J-P, Lavaysse C, Lebel T, Marticorena B, Mounier F, Redelsperger J-L, Reeves C, Roca R, de Rosnay P, Sultan B, Thorncroft CD, Tomasini M. 2008. Large-scale overview of the summer monsoon over West and Central Africa during the AMMA field experiment in 2006. *Ann. Geophys.* **26**: 2569–2595.
Kaiser JF, Reed WA. 1977. Data smoothing using low-pass digital filters. *Rev. Sci. Instrum.* **48**: 1447.
Kållberg P, Berrisford P, Hoskins BJ, Simmons A, Uppala S, Lamy-Thépaut S, Hine R. 2005. *ERA-40 Atlas*. *ERA-40 Project Report Series* No. 19. ECMWF: Reading, UK.
Kiladis GN, Weickmann KM. 1997. Horizontal structure and seasonality of large-scale circulations associated with submonthly tropical convection. *Mon. Weather Rev.* **125**: 1997–2013.
Knippertz P. 2005. Tropical–extratropical interactions associated with the Atlantic tropical plume and subtropical jet streak. *Mon. Weather Rev.* **133**: 2759–2776.
Knippertz P, Martin JE. 2005. Tropical plumes and extreme precipitation in subtropical and tropical West Africa, *Q. J. R. Meteorol. Soc.* **131**: 2337–2365.
Knippertz P, Fink AH, Reiner A, Speth P. 2003. Three late summer/early autumn cases of tropical-extratropical interactions causing precipitation in Northwest Africa. *Mon. Weather Rev.* **131**: 116–135.
Lavaysse C, Diedhiou A, Laurent H, Lebel T. 2006. African easterly waves and convective activity in wet and dry sequences of the west African monsoon. *Clim. Dyn.* **27**: 319–332.
Lavaysse C, Flamant C, Janicot S, Parker DJ, Lafore J-P, Sultan B. 2009. Seasonal evolution of the West African heat low: A climatological perspective. *Clim. Dyn.* **33**: DOI: 10.1007/s00382-009-0553-4.
Lebel T, Parker DJ, Flamant C, Bourles B, Marticorena B, Mougin E, Peugeot C, Diedhiou A, Haywood J, Ngamini JB, Polcher J, Redelsperger J-L, Thorncroft CD. 2009. The AMMA field campaigns: Multiscale and multidisciplinary observations in the West Africa region. *Q. J. R. Meteorol. Soc.* **136**(s1): 8–33.
Leroux S, Hall NJ. 2009. On the relationship between African Easterly Waves and the African Easterly Jet. *J. Atmos. Sci.* **66**: 2303–2316.
Matthews A. 2004. Intraseasonal variability over tropical Africa during northern summer. *J. Climate* **17**: 2427–2440.
Mathon V, Laurent H, Lebel T. 2002. Mesoscale convective system rainfall in the Sahel. *J. Appl. Meteorol.* **41**: 1081–1092.
Nicholson SE. 1981. Rainfall and atmospheric circulation during drought periods and wetter years in West Africa. *Mon. Weather Rev.* **109**: 2191–2208.
Parker DJ, Thorncroft CD, Burton R, Diongue-Niang A. 2005. Analysis of the African easterly jet, using aircraft observations from the JET 2000 experiment. *Q. J. R. Meteorol. Soc.* **131**: 1461–1482.
Porcu F, Carrassi A, Medaglia CM, Prodi F, Mugnai A. 2007. A study on cut-off low vertical structure and precipitation on the Mediterranean region. *Meteorol. Atmos. Phys.* **96**: 121–140.
Ramel R, Gallée H, Messager C. 2006. On the northward shift of the West African monsoon. *Clim. Dyn.* **26**: 429–440.
Redelsperger J-L, Thorncroft CD, Diedhiou A, Lebel T, Parker DJ, Polcher J. 2006. African Monsoon Multidisciplinary Analysis: An international research project and field campaign. *Bull. Am. Meteorol. Soc.* **87**: 1739–1746.
Smith RK, Reader MJ, Tapper NJ, Christie DR. 1995. Central Australian cold fronts. *Mon. Weather Rev.* **123**: 16–38.
Spengler T, Smith RK. 2008. The dynamics of heat lows over flat terrain. *Q. J. R. Meteorol. Soc.* **134**: 2157–2172.
Spengler T, Reeder MJ, Smith RK. 1995. The dynamics of heat lows in simple background flows. *Q. J. R. Meteorol. Soc.* **131**: 3147–3165.
Sultan B, Janicot S, Diedhiou A. 2003. The West African Monsoon dynamics. Part I: Documentation of intraseasonal variabilty. *J. Climate* **16**: 3389–3406.
Thorncroft CD, Blackburn M. 1999. Maintenance of the African easterly jet. *Q. J. R. Meteorol. Soc.* **125**: 763–786.
Thorncroft CD, Flocas HA. 1997. A case study of Saharan cyclogenesis. *Mon. Weather Rev.* **125**: 1147–1165.
Torrence C, Compo GP. 1998. A pratical guide to wavelet analysis. *Bull. Am. Meteorol. Soc.* **79**: 61–78.
Trenberth KE, Stepaniak DP, Caron JM. 2000. The global monsoon as seen through the divergent atmospheric circulation. *J. Climate* **13**: 3969–3993.
Viltard A, de Félice P, Oubuih P. 1997. Comparison of the African and the 6–9 day wave-like disturbance pattern over West Africa and the tropical Atlantic during summer 1985. *Meteorol. Atmos. Phys.* **62**: 91–99.
Vizy EK, Cook KH. 2009. A mechanism for African monsoon breaks: Mediterranean cold air surges. *J. Geophys. Res.* **114**: DOI: 10.1029/2008JD010654.
Zhang C, Woodworth P, Gu G. 2006. The seasonal cycle in the lower troposphere over West Africa from sounding observations. *Q. J. R. Meteorol. Soc.* **132**: 2561–2584.

